("BOSS" Conference, Trondheim, Norway, June 1988)

THE COMPUTATION OF WAVE LOADS ON LARGE OFFSHORE STRUCTURES

J. Nicholas Newman
Paul D. Sclavounos

Department of Ocean Engineering
Massachusetts Institute of Technology
Cambridge, MA 02139

USA

ABSTRACT

The reliable analysis of wave interactions with large offshore structures of complex form requires a robust and accurate numerical solution of the linearized radiation/diffraction problems. A new panel program is described which has been developed for this purpose, based on the application of Green's identity to obtain an integral equation for the velocity potential on the body surface. Important features of the program are controlled accuracy, fast evaluation of the wave-source potential, and an accelerated iterative solver which permits the use of large numbers of panels. Illustrative computations are presented for a TLP and a catamaran-barge configuration with a small gap between the two hulls. Possible future developments in this field are suggested, and the validation of computer programs is emphasized.

1. INTRODUCTION

Following the pioneering development of 'panel' methods for aerodynamic flows by Hess and Smith [1], several programs have been developed to analyze water-wave radiation and diffraction, using distributions of sources on the submerged body surface and solving a linear system of equations for the unknown source strength on each panel. Early applications used computationally intensive algorithms for the free-surface source potential, or 'Green function'. This restricted both the number of panels used to discretize the structure and the number of separate computations used to characterize the frequency response and dependence on geometric parameters. Moreover, it was not generally feasible to use a sufficiently large number of panels to test for numerical convergence. The last shortcoming was less apparent when 'compact' bodies of simple geometrical form were studied, and when the validation of the programs was based on experimental data, but more extensive computations and comparisons for practical offshore structures have revealed substantial uncertainties.

An example is provided by the ISSC comparison of results from 17 different radiation/diffraction programs for the TLP shown in Figure 1. The results of this comparison are summarized by Eatock Taylor and Jefferys [2], and the surge added mass is re-plotted in Figure 2. Most of these results are based on panel programs, using discretizations with a few hundred panels. A substantial scatter exists even in the long-wavelength regime.

Also included in Figure 2 are our own more recent results for the same TLP, based on the program WAMIT. The solid curve shows our principal results obtained with 1928 panels, using forty periods to define the complicated frequency-dependence associated with wave interference

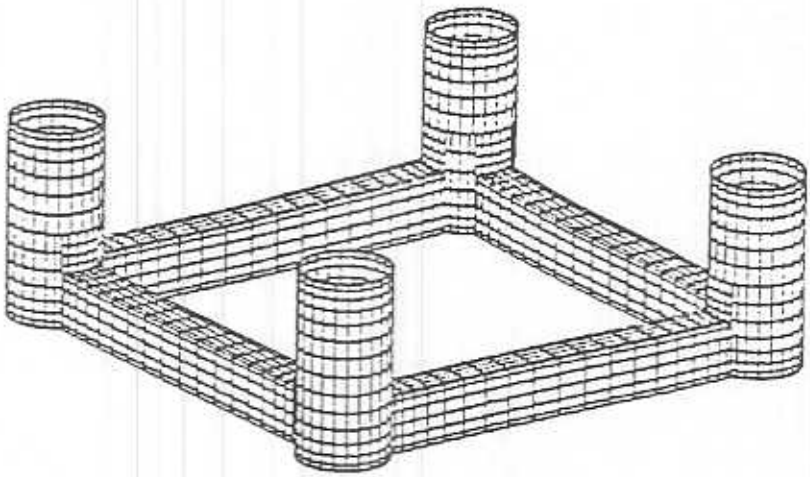

Figure 1 – Submerged surface of the ISSC TLP represented by 4096 panels.

between the TLP columns. To indicate the sensitivity to the number of panels, seven more accurate computations are shown with 4048 panels, and less accurate results obtained with 512 panels are indicated by the broken curve. Collectively these three sets of data imply convergence at a level 1-2% below the solid curve.

All of the results plotted in Figure 2 are based on the same linear potential-flow model, which is well accepted and unambiguous. The variations among different programs must therefore be attributed to some combination of errors in the programs, or in their use. Various explanations have been offered including improper discretizations of the body, and inaccurate evaluations of the influence functions (integrals over each panel of the source potential and its normal derivative). Assuming the correctness of our own extrapolated results, only four of the other seventeen sets of data lie within 10% of this benchmark.

In the present paper we describe some features of the three-dimensional free-surface panel program, WAMIT (WaveAnalysisMIT), which has been developed in response to the perceived need for more accurate and efficient programs in this field. Particularly important in this development are special algorithms and subroutines for the evaluation of the influence functions, and a unique iterative solver for the linear system of equations. Collectively these features make it possible to analyze structures which are represented by thousands, rather than hundreds, of panels, and to do so with controlled accuracy.

Preliminary results for idealized body shapes were presented at the last BOSS Conference [3], including comparisons with benchmark computations derived from an independent curvilinear-panel program. Subsequently, WAMIT has been developed for use with offshore structures of practical form, and several options have been implemented to permit the evaluation of first-order hydrodynamic forces, body motions in waves, pressures on the body, pressures and/or velocities in the fluid domain, and second-order drift forces. Several of these capabilities have been illustrated for a six-column TLP [4] using up to 12,608 panels to demonstrate convergence, and the results have been confirmed with a complementary time-domain panel program.

After reviewing the development of WAMIT results will be presented for a particularly difficult configuration, consisting of two rectangular barges separated by a small gap. In Section 7 we speculate on future developments in this field, associated with the use of parallel processors, and in the concluding Section 8 special attention is given to the validation of computer programs.

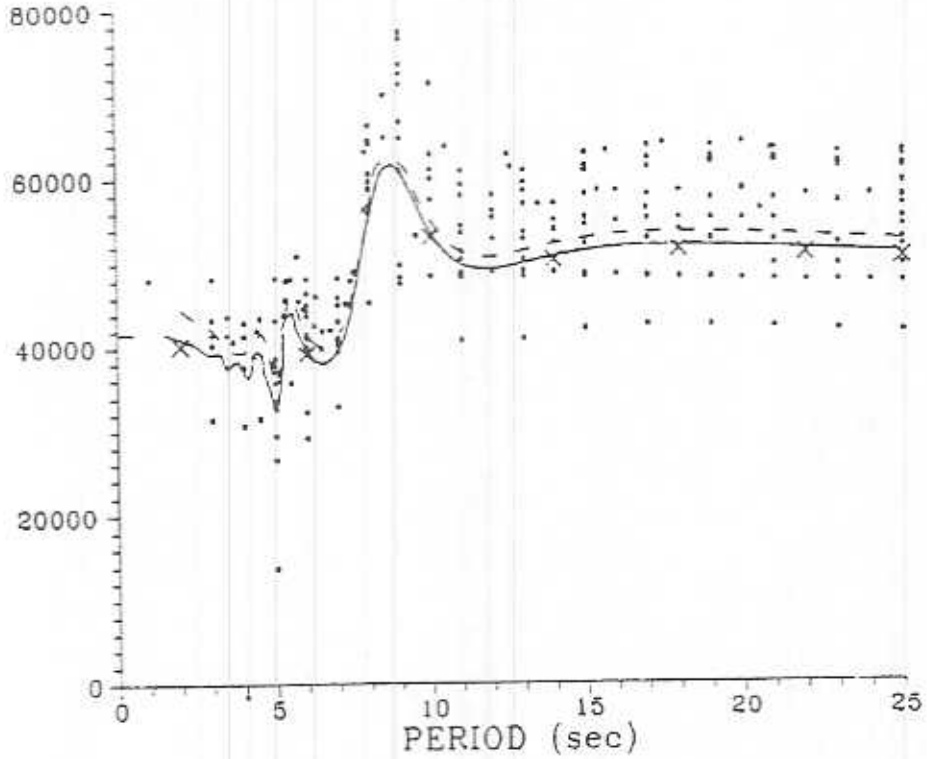

Figure 2 – Surge added mass of the ISSC TLP. The solid curve is evaluated by WAMIT using 1928 panels and 40 closely-spaced frequencies. The tick-mark on the ordinate indicates the limiting value 41633 for a period of zero, derived from the time-domain analysis of Korsmeyer [4] using the same discretization. Analogous results with 4096 panels are indicated by the symbols (×), and with 512 panels by the broken curve. The symbols (∗) denote computations from other programs as summarized by Eatock Taylor and Jefferys [2]. The results shown are dimensional, as defined in [2].

2. THE INTEGRAL EQUATIONS

The radiation and diffraction problems in the frequency domain correspond respectively to forced motions of the structure in calm water, and to the interaction of a fixed structure with incident regular waves. Both problems are subject to the Laplace equation in the fluid domain, the linearized free-surface condition, the no-flux condition through the bottom of the fluid, appropriate Neumann conditions on the mean position of the body wetted surface, and the radiation condition at infinity.

We adopt the complex time factor $e^{i\omega t}$, which is assumed to apply hereafter. The potential for a unit source, in the absence of the body, defines the Green function G which is well known [5]. This fundamental solution is used with Green's theorem to derive an integral equation for the velocity potential on the body surface S,

$$2\pi\phi(\mathsf{x}) + \iint_S \phi(\xi)\frac{\partial G}{\partial n_\xi}\,d\xi = \iint_S V(\xi)G\,d\xi, \tag{1}$$

where the normal velocity $V(\xi)$ is prescribed on S.

In the diffraction problem we define $\phi = \phi_D = \phi_I + \phi_S$ to be the total velocity potential, where ϕ_I is the specified incident-wave and ϕ_S the scattered potential. The boundary condition is $\partial\phi_D/\partial n = 0$ on S. The integral equation (1) can be applied directly to ϕ_S, with the result

$$2\pi\phi_S(\mathbf{x}) + \iint_S \phi_S(\xi)\frac{\partial G}{\partial n_\xi}\,d\xi = \iint_S \frac{\partial \phi_S}{\partial n_\xi} G\,d\xi \tag{2}$$

Alternatively, if Green's theorem is applied to ϕ_I on the *interior* of S, with the field point $\mathbf{x}$ on the same surface, it follows that

$$-2\pi\phi_I(\mathbf{x}) + \iint_S \phi_I(\xi)\frac{\partial G}{\partial n_\xi}\,d\xi = \iint_S \frac{\partial \phi_I}{\partial n_\xi} G\,d\xi \tag{3}$$

(The interior space is appropriate in this application since ϕ_I is harmonic throughout the half-space beneath the plane of the free surface, whereas this potential does not satisfy the radiation condition in the far-field. The only formal change in the integral equation is in the direction of the normal vector, which is defined consistently to be positive out of the fluid domain and into the body.) Equations (2) and (3) can be combined, and after invoking the boundary condition on the body surface the simpler integral equation

$$2\pi\phi_D(\mathbf{x}) + \iint_S \phi_D(\xi)\frac{\partial G}{\partial n_\xi}\,d\xi = 4\pi\phi_I(\mathbf{x}) \tag{4}$$

is derived for the diffraction potential.

In WAMIT the integral equations (1) and (4) are solved for the velocity potentials of the radiation and diffraction problems, respectively. This approach is somewhat different from the more common source-formulation, inwhich an integral equation is solved for the unknown source strength and the velocity potential is obtained subsequently by another integration.

Before discussing the numerical analysis it should be noted that the solutions of these integral equations are not unique at a set of 'irregular frequencies'. This has been a troublesome issue in the development of panel programs, and significant errors have been observed in some cases. Following analogous work in acoustics [6], a method has been developed [7,8,9] to remove the error due to all irregular frequencies. This method is based on the solution of a modified integral equation for the velocity potential over the body surface. A discussion of the manifestation, importance and removal of irregular-frequency effects is given in [4]. For most offshore structures the irregular frequencies do not appear to be of practical importance, particularly when the formulation (1-4) is used rather than the alternative of solving for an unknown source distribution.

The integral equations (1) and (4) are discretized by subdividing S into an ensemble of N panels s_j, assuming a constant potential ϕ_j and normal velocity V_j on each panel, and enforcing the equation at the panel centroids. For the radiation potentials it follows that

$$2\pi\phi_i + \sum_{j=1}^{N}\phi_j \iint_{s_j}\frac{\partial G}{\partial n_\xi}\,d\xi = \sum_{j=1}^{N} V_j \iint_{s_j} G\,d\xi \tag{5}$$

A similar equation follows from (4) for the diffraction potential. The result is a system of N complex linear algebraic equations with the same number of unknowns.

Each panel s_j is defined by the offsets of its four vertices. A triangle is obtained in the special case of two coalescent vertices. When the four vertices of a panel are not co-planar, it is customary to define a plane which in some sense is a best fit to these vertices; we exploit the geometric property that the midpoints of the four sides of any quadrilateral lie in the same plane. The projection of the four vertices onto this plane defines the *plane panel* used for the discrete analysis. (The plane panel defined in this manner is identical to that which is obtained by Hess and Smith [1] following a slightly different procedure.)

In computations based on this formulation, the two principal tasks are: (a) the evaluation of the hydrodynamic influence coefficients for all panels, which involves $O(N^2)$ evaluations of the Green function; and (b) the solution of a dense complex linear system of order N, which involves $O(N^3)$ floating-point operations if carried out by Gauss reduction and $O(N^2)$ operations if carried out by an iterative method. These tasks are discussed in Sections 3-4.

3. SET-UP OF THE MATRIX

The matrix coefficients are constructed by integration of the Green function and its normal derivative over each panel. For this purpose the Green function is decomposed into Rankine singularities (the basic $1/R$ singularity, its image above the free surface and, in finite depth, its image below the bottom of the fluid domain), a logarithmic singularity which is significant if the source and field point are close to each other and to the free surface, and the bounded remainder required to satisfy the free-surface boundary condition. Special attention is given to each of these components.

For the Rankine influence coefficients, the analytical procedure of Hess and Smith [1] has been extended [10] to provide robust algorithms, for all possible positions of the field point relative to the panel, with a uniform tolerance of six decimals accuracy. When the field point is sufficiently far from the panel a fourth-order multipole approximation is employed.

Analogous analytical techniques have been derived for the logarithmic singularity, as summarized in the Appendix. Our experience has shown that the analytic integration of the logarithmic singularity may be significant when studying run-up, or other features of the solution near the intersection of the body and the free surface.

The above components, which are independent of frequency, may be evaluated once and stored for subsequent use to minimize their computational burden.

Efficient algorithms for the evaluation of the free-surface component of the Green function have been developed [11] and coded in the subroutine FINGREEN. Numerical experiments confirm that a single-node centroid integration provides an accuracy which is consistent with the discretization error introduced by the approximation of the geometry and the velocity potential. The single-node quadrature formula allows the use of the symmetry properties of the Green function to evaluate the two matrix coefficients corresponding to a pair of panels with one call to FINGREEN, thus requiring $N^2/2$ total calls for a body with no planes of symmetry.

For bodies with one or two planes of symmetry, the input panels may be distributed over half or a quarter of the body, and both the number of evaluations of the Green function and the dimension of the linear system are reduced by factors of two or four, respectively.

4. SOLUTION OF THE LINEAR SYSTEM

Direct Gauss reduction is the conventional method of solution for the complex, dense linear system (5), and its counterpart in the diffraction problem. Unless special steps are taken to implement an out-of-core solver, this method of solution is sensitive to the RAM capacity of the machine being used. A more fundamental difficulty is that this solution method requires a computational effort proportional to N^3, and it is not feasible to use panel numbers substantially greater than 1000. On the other hand, an advantage of the direct method of solution is that the effort to reduce the solution matrix is practically independent of the number of right-hand side vectors, i.e. the number of modes analyzed in the radiation problem and the number of wave headings in the diffraction problem. Version 1 of WAMIT is based on this approach with a conventional Gauss factorization and back-substitution.

To overcome the $O(N^3)$ computational burden of the direct method of solution, an iterative solver has been developed and implemented in Version 2 of WAMIT. This solution technique is based on the Gauss-Siedel method, accelerated by a conjugate-gradient algorithm. The convergence test is based on a tolerance of six decimals in the residual-error norm. For various body geometries including four- and six-column TLP's, convergence generally is achieved in 10-15 iterations. Larger numbers of iterations have been observed in special cases where the matrix is poorly conditioned, due either to proximity to an irregular frequency, or to a physical resonance which is highly-tuned. An example of the latter type is discussed in Section 6.

The principal advantage of the iterative solution is that the computational effort is proportional to N^2. Moreover, the matrix elements can be stored out-of-core in a manner which permits fast sequential transfer. For this reason the iterative solver is especially suitable for implementation on small computer systems such as PC's. The results presented in this paper are based entirely on the iterative method of solution, and most of these results have in fact been obtained on a PC-AT microcomputer system.

To compare the efficiency of the direct and iterative solvers, we shall consider a typical run involving several frequencies or wave periods. In this context one can ignore the time required to evaluate the panel geometric parameters and Rankine matrix coefficients, which are stored for subsequent use at each frequency. The only significant computational burden in the solution is then associated with (a) the evaluations of the free-surface Green function (and its gradient), and (b) the solution of the linear system for each specified radiation or diffraction mode. Table 1 indicates the approximate time required for each of these tasks on a VAX 11-750 minicomputer. The performance of larger minicomputer systems and mainframes is substantially faster, but the relative burden of each task should be similar on all serial computers. On vector machines such as the Cray, where it is feasible to vectorize the direct and iterative solvers, the computational burden of task (b) is reduced relative to (a) by an order of magnitude.

When Gauss reduction is used, the relative burden between the set-up and solution depends on the number of panels. The first two rows in Table 1 indicate that these two tasks require approximately equal time if the total number of panels is of order 100 with no planes of symmetry, 400 with one plane of symmetry, and 1600 with two planes of symmetry. Thus the number of planes of symmetry affects this comparison significantly.

When the iterative solver is used, both tasks are quadratic in N and their relative magnitudes are roughly the same. However, this comparison is for infinite depth and based on a serial computing system. Finite depth increases the burden of the Green function evaluation by a factor of 2-4, and vectorized evaluation of the solver may reduce the time for task (b) substantially. Thus the evaluation of the Green function remains the most critical aspect of the overall problem.

Planes of Symmetry:	0	1	2
Set-up (Green function)	1.2 N^2	0.6 N^2	0.3 N^2
Direct solution	0.0128 N^3	0.0016 N^3	0.0002 N^3
Iterative (1 mode)	0.96 N^2	0.24 N^2	0.06 N^2
Iterative (6 modes)	5.76 N^2	1.44 N^2	0.36 N^2

Table 1 – Approximate CPU times in milliseconds for set-up and solution of the linear system on a VAX 11/750 system. N = total number of panels. Times for the Green function evaluation are for infinite fluid depth. Times for the direct solution do not include overhead when the number of unknowns is large in relation to the available RAM.

5. CONVERGENCE AND VALIDATION

For a boundary surface with continuous curvature, the combination of plane panels with a constant value of the velocity potential on each panel involves discretization errors of the same order. This 'optimal' combination is also 'consistent', because the error can be shown to vanish in the limit $N \rightarrow \infty$. However, these properties are not sufficient to ensure that the discrete solution will converge to its continuous limit. For example, it is possible that inaccurate integrations of the Rankine singularity for neighboring panels will generate inconsistent approximations of the influence coefficients, leading to a solution of (5) which with increasing N may converge to the wrong answer. For this reason a conservative tolerance of six decimals has been used in WAMIT, not only for the panel integration of the Rankine singularities, but also in the FINGREEN subroutine for the free-surface source potential.

Rational estimates of the rate of convergence are not available. For a variety of structures, evaluations of the hydrodynamic forces and free-surface elevations with WAMIT indicate that convergence is achieved with increasing numbers of panels. For bodies with sharp corners we find that the rate of convergence is affected significantly by the spacing of panels near the corners.

Confidence that the converged solution is in fact correct requires several validation tests. The first tests of WAMIT were based on studies of simple body shapes including spheres, spheroids, and axisymmetric cylinders [3]. Convergence tests and extrapolated results were made, together with comparisons with benchmarks from independent programs and other works. Validation for more complicated structures has been performed subsequently, notably in the analysis of a six-column TLP [4]. The latter work includes convergence tests with up to 12,608 panels, and comparison of the (frequency-domain) added-mass and damping coefficients with Fourier transforms of the time-domain impulse-response function for the same structure.

6. COMPUTATONAL RESULTS FOR A CATAMARAN BARGE

To illustrate some of the results from WAMIT in a relatively difficult application, we consider two rectangular barges arranged in a catamaran configuration and separated by a small gap, as shown in Figure 3. The length, beam and draft of each barge are L = 80m, B = 20m, T = 10m, respectively, and the gap width is 4m.

This type of configuration is notable from the standpoint of the resonant motion which occurs in the gap when the product of the wavenumber and draft is near unity [12]. Most numerical studies of this phenomenon are two-dimensional (cf. Marthinsen and Vinje [13], who also consider the effects of viscosity and nonlinearity near the resonant frequency). Analogous problems arise in the analysis of a monohull with an internal 'moon pool'.

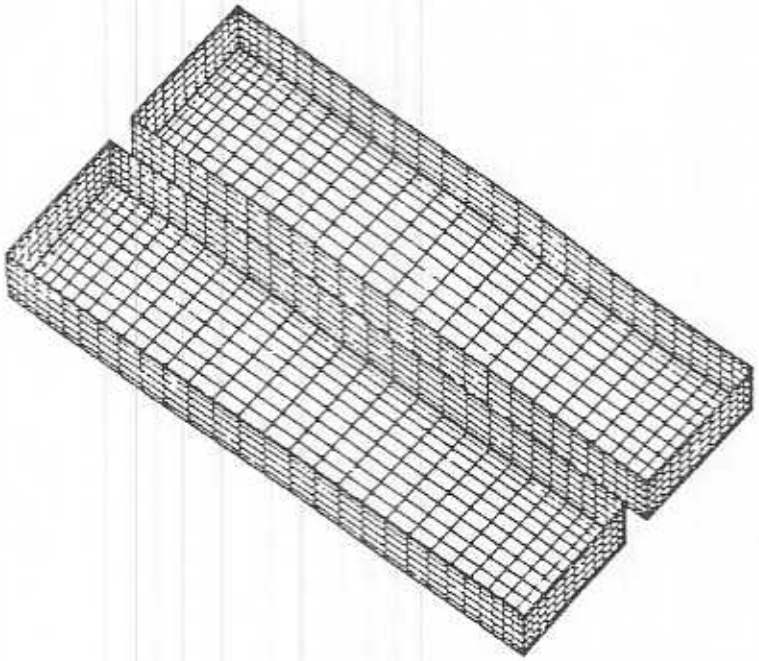

Figure 3 – Catamaran barge discretized with a total of 2560 panels. The dimensions of each barge are $L = 80$m length, $B = 20$m beam, $T = 10$m draft, and the gap is 4m wide.

We restrict our discussion here to forced heave and pitch motions in calm water, since these separate modes illustrate the gap resonance more clearly than when the motions are superposed with the diffraction problem. In the three-dimensional analysis two discretizations are employed, with the total number of panels on both barges equal to 640 and 2560 respectively. The latter discretization is illustrated in Figure 3. The discretizations used here are based on 'cosine' distributions, to provide a finer spacing near the corners and also near the free surface. In the Figures which follow, the curves are based on the coarse discretization, and discrete points are used to denote the more accurate results with smaller panels.

Before considering the three-dimensional analysis it is instructive to present results from the analogous problem in two dimensions. Figure 4 shows the strip-theory approximation for the added mass and damping, obtained from the two-dimensional program NIIRID, a potential-based integral-equation program analogous to WAMIT. The resonant gap oscillation at a period of 7.7 seconds is pronounced in this Figure. A small effect also is apparent from the first irregular frequency at 4.8 seconds. In the results shown by the solid curve, the body section is represented by a total of 32 segments (16 for each rectangular hull). More accurate results with a total of 64 segments are shown to indicate the convergence. These two representations are identical at each section to the corresponding discretizations used in three dimensions.

Figure 5 shows three-dimensional results from WAMIT for the added mass and damping. The coarse discretization appears to be sufficiently accurate for most practical purposes. As in the analogous results for an axisymmetric cylinder [4], the bandwidth of the irregular-frequency effect is reduced by increasing the number of panels.

In Figure 6 the free-surface elevation is shown at three longitudinal positions within the gap including the center ($x = 0$), half way to the ends ($x = \pm L/4$), and at the ends ($x = \pm L/2$). (From symmetry the free-surface elevation associated with the pitch mode is zero at the center.) At most periods the elevation is a maximum in the middle, decreasing toward the ends of the

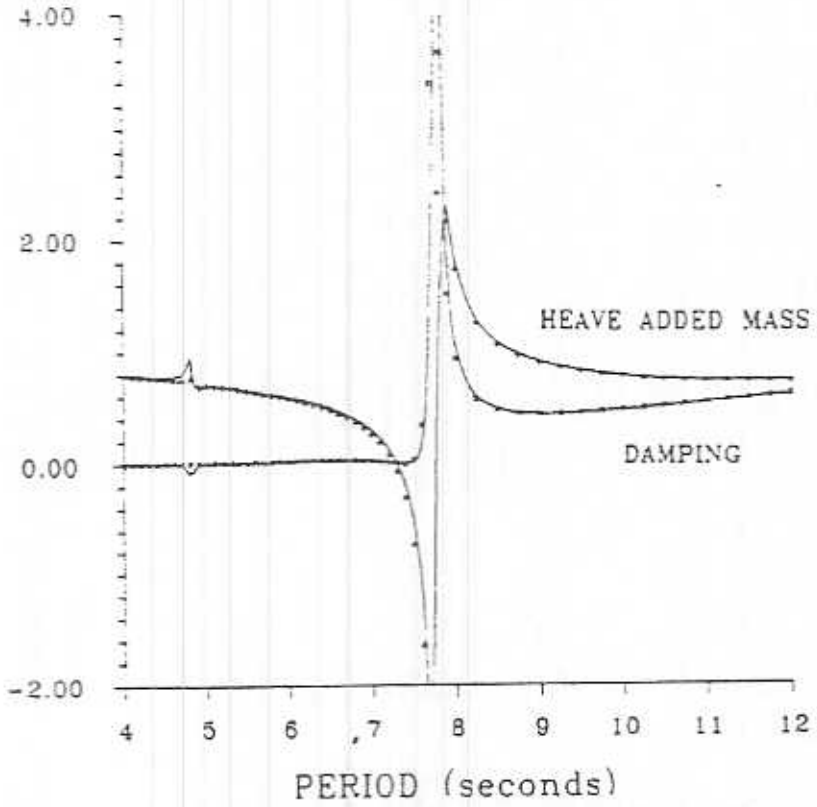

Figure 4 – Strip-theory approximation to the added mass and damping of the catamaran barge. The solid curves are based on discretization with 32 segments on the cross-section of the two hulls, and the marks (+, ×) are with 64 segments. The results are nondimensionalized based on the length scale $L/2$, frequency, and the fluid density.

gap. The resonance is pronounced, with a predicted free-surface elevation at the center 50 times the heave amplitude. The effects of both the gap resonance and the irregular frequencies are magnified here, by comparison to the integrated coefficients in Figure 5.

Comparison of Figures 4-5 reveals that the magnitude of the gap resonance is substantially reduced by three-dimensional effects, and the resonant periods are shifted downward. Thus it is not appropriate to analyze this type of configuration with a strip-theory approach. We shall discuss the resonant periods further after first analyzing the irregular frequencies.

The irregular frequencies for multiple floating bodies can be predicted from the eigensolutions of the free-surface problem in the interior of each separate body [4]. The values for a rectangular barge are easily evaluated by separation of variables. Since the solutions of the heave and pitch radiation problems are symmetric and antisymmetric, respectively, the corresponding eigensolutions are

$$\phi = \begin{matrix}\cos\\ \sin\end{matrix}(k_x x)\cos(k_y y)\sinh(k(z+T)) \qquad (6)$$

Here (k_x, k_y) denote the components of the wavenumber with scalar length k, T is the draft, and the origin is at the center of the rectangular waterplane. Antisymmetric modes in y, which correspond to relatively high irregular frequencies beyond the range shown in Figures 4-6, are ignored in this discussion.

The discrete values of (k_x, k_y) are determined by requiring the potentials (6) to vanish on $y = \pm B/2$ and $x = \pm L/2$, and the irregular frequencies follow from the free-surface condition, $K \equiv \omega^2/g = k\coth(kT)$. For the two-dimensional case shown in Figure 4, with $k_x = 0$, the

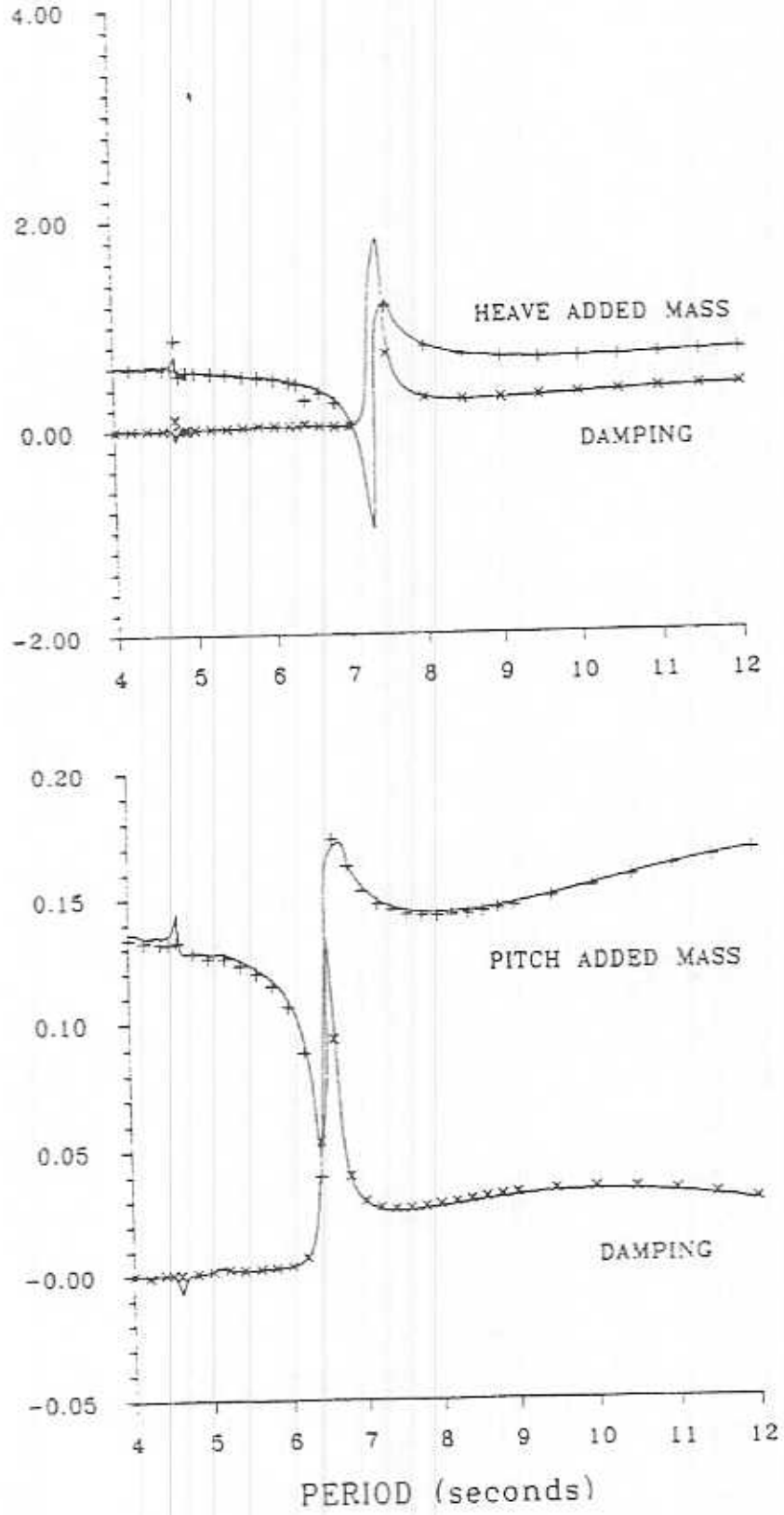

Figure 5 – Added mass and damping of the catamaran barge. The solid curves are based on discretization with a total of 640 panels for both hulls, and the marks (+, ×) are computed with 2560 panels. The results are nondimensionalized based on the length scale $L/2$, frequency, and fluid density.

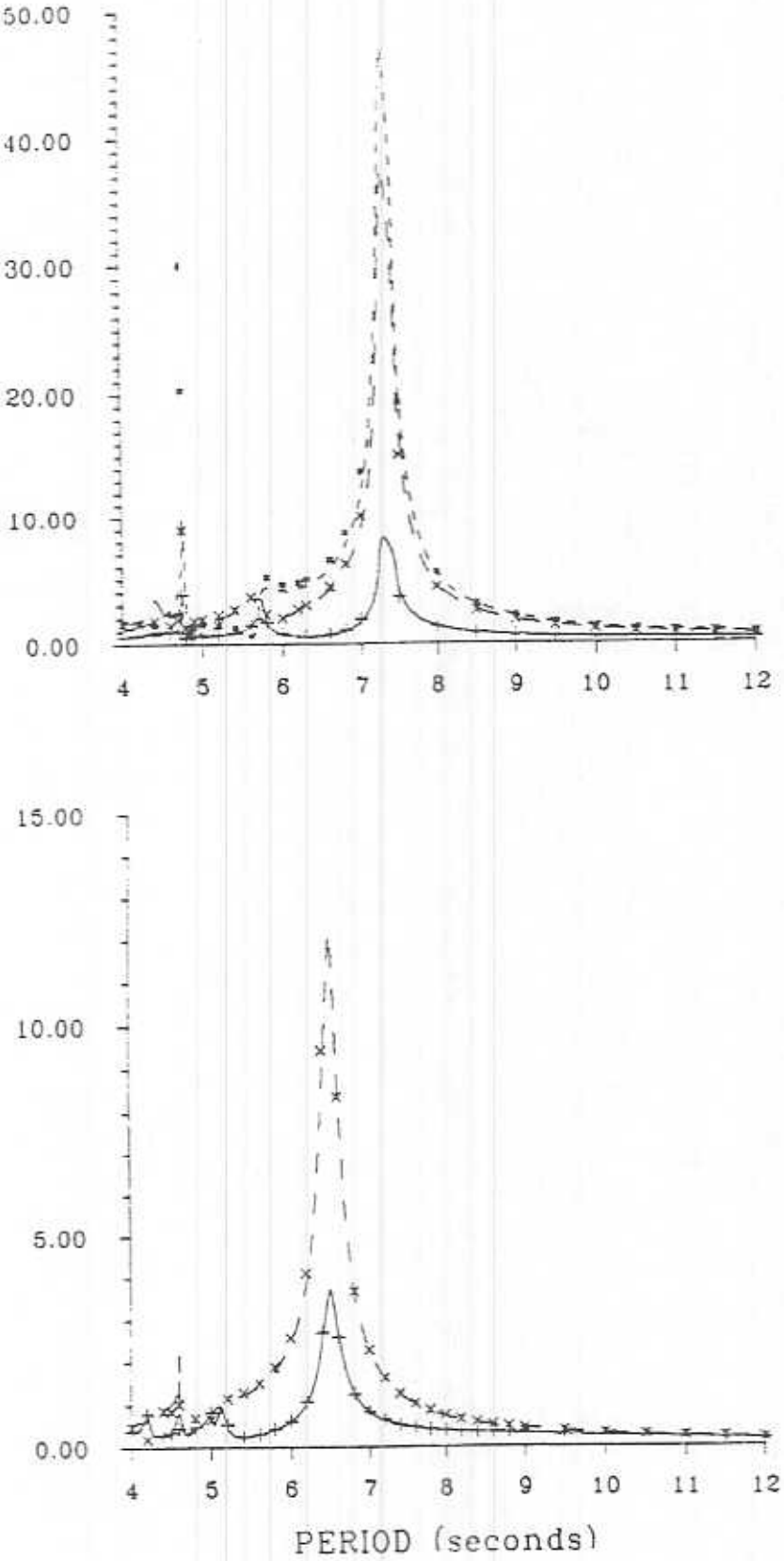

Figure 6 – Free-surface elevation in the gap. Three positions on the free surface are shown on the centerline: (- - - -) denotes the midpoint of the gap ($x = 0$), (– – – –) denotes positions half way toward each end ($x = \pm L/4$) and (——) denotes the ends of the gap ($x = \pm L/2$).

lowest irregular frequency for the indicated dimensions corresponds to $k = k_y = \pi/B$, and thus to a period of 4.85 seconds. In three dimensions the same value applies for k_y, and the lowest irregular frequency for heave occurs when $k_x = \pi/L$, with the period 4.79 seconds. For pitch the corresponding values are $k_x = 2\pi/L$ and 4.65 seconds. These periods are consistent with the computational results in Figures 4-6.

A similar analysis applies to the gap resonances, but with important distinctions. Unlike the irregular frequencies, which are present only in the mathematical solution of the integral equation, resonant motions in the gap are physically real, although generally exaggerated by the assumptions of linear potential theory. The other important difference is that the resonant modes in the gap must satisfy homogeneous Neumann boundary conditions on the sides, rather than Dirichlet conditions. Two-dimensional standing-waves with $k_y = 0$ are the most important modes when the gap width is small.

The common feature of the irregular-frequency and resonant-gap modes is that homogeneous Dirichlet conditions apply on the boundaries $z = -T$ and $x = \pm L/2$, under the assumption that the gap width is small. To see this analogy we recall and generalize the two-dimensional analysis [12], based on the method of matc' asymptotic expansions. Three regions of the flow are significant including (a) the interic ie gap, (b) an intermediate domain near the entrance to the gap, and (c) the exterior fl ociated with the remainder of the body and the free surface. Resonance is possible if the a nontrivial solution in the gap with zero (or asymptotically small) value in the exterior re.n. For example, the purely vertical gap motion $\phi = Kz + 1$ satisfies the free-surface condition, and vanishes when $z = -T$ if $KT = 1$. Since matching of the (narrow) gap flow to the exterior domain is carried out within a small distance of the latter point, it is possible in the asymptotic analysis to match a large gap motion to a relatively small exterior flow when $KT \simeq 1$.

For T =10m this simplified analysis implies resonance at 6.3 seconds, but the added mass of the fluid in the intermediate domain effectively increases the draft, by an amount of the same order as the gap width. If the conformal-mapping analysis of Marthinsen and Vinje [13] is applied to the present geometry, the effective draft is increased by 3.0m to a total of 13.0m; on this basis the resonant period is increased to 7.2 seconds. The resonance in Figure 4 at 7.7 seconds implies a somewhat larger effective draft of 14.7m, which may be due to the fact that the ratio of the draft to the gap width is not sufficiently large to make the simplified analysis accurate.

Similar arguments apply to the three-dimensional problem, based on the solutions (6) with $k_y = 0$, and with the draft increased to account for the added-mass effect. (A similar effective lengthening of the gap at the ends $x = \pm L/2$ has little effect on the resonant periods.) Using the effective draft of 14.7m, we find the first three symmetric modes for heave to be at periods of 7.3, 5.7, and 4.5 seconds. The corresponding antisymmetric pitch modes are at 6.5, 5.0, and 4.1 seconds. The first two periods for each mode are apparent in Figure 5. The shorter periods are obscured within the band of irregular frequencies. Only the first resonant mode has a significant effect on the integrated heave force or pitch moment.

7. FUTURE PROSPECTS - VECTORIZATION AND PARALLEL PROCESSING

Future developments of the panel method can be anticipated to take advantage of present and future computing systems, particularly vector supercomputers and parallel processors. If the iterative method of solution is employed, the balance between the set-up and solution is independent of the number of panels, and our principal concern is to increase the computational speed of setting up the influence coefficients.

The vectorization of FINGREEN has been considered for both the finite- and infinite-depth cases, which must be considered separately in this context. Some possibilities exist in this direction, which could substantially reduce the computing time on specific systems such as the Cray, but significant programming effort and algorithm development is required to approach full vectorization.

The alternative of parallel processing appears more attractive, since it does not require substantial re-programming, and the same parallelism can be exploited in both the Rankine and free-surface elements. The conversion of a sequential to a parallel algorithm for implementation on a system with a large number of processors aims at achieving the highest degree of concurrency during the computation. On a system with M processors, the maximum possible speed-up of a computational task is a factor of M relative to the effort on a single processor. In practice, the speed-up is ϵM, where $\epsilon < 1$ because of the inter-processor communication overhead which depends on the architecture of the parallel processor and the algorithm used for the solution of the problem at hand.

In the water-wave radiation/diffraction problem efficient algorithms for the set-up of the influence matrix on parallel processors may be similar to algorithms suggested for the treatment of the gravitational attraction of a large number of bodies [14]. High efficiencies ϵ can be achieved on parallel processors with architectures based on shared or distributed memory, if the processors are connected in a ring topology which permits each node to communicate with the two adjacent neighbors. Partitioning the evaluation of matrix elements among the available M processors, it follows that

$$\epsilon \approx 1 - \frac{M}{N} \frac{t_{comm}}{t_{eval}} \tag{7}$$

where t_{comm} is the time required for communication between two processors and t_{eval} the time to evaluate the influence coefficient. The computational burden of the influence coefficients implies that $t_{comm} << t_{eval}$, and if the number of panels N is comparable to or greater than the number of processors M a high efficiency can be achieved in the set-up of the matrix.

8. CONCLUSIONS

We have shown that it is possible to analyze wave effects on large offshore structures with a high degree of accuracy, efficiency, and confidence. Particularly important in this respect is the ability to make computations for practical structures with a sufficiently large number of panels to demonstrate numerical convergence. This by itself does not guarantee correctness of the program, however.

The validation of computer programs is a topic of universal importance, which lately has received attention in the ITTC and other forums. In addition to the verification of numerical convergence, careful and systematic validation requires a variety of other tests including comparison with recognized analytic results, and with independent computations for more complicated applications where no analytic results exist.

Tests also should be made in special cases where the theory provides redundant checks, such as the symmetry of cross-coupling coefficients or the use of the Haskind relations to compare with direct evaluation of the exciting forces. These tests are simple to implement, and provide good estimates of the maximum accuracy to be expected, but they are not sufficient by themselves to validate a program. Also useful are qualitative comparisons with asymptotic approximations, as in our analysis of the small-gap problem in Section 6. Finally, the program should be tested with special attention in regimes where it may not be reliable, such as the vicinity of the irregular frequencies.

Notably absent from our discussion is validation based on comparisons with experimental data. It is vitally important to validate any *theory* by comparison to experiments or full-scale measurements, so that the limitations and assumptions are defined to the maximum extent possible. But programs based on unambiguous and well established theories must be held to a higher level of accuracy than can be achieved in most experiments.

To be more specific in the context of wave loads on offshore structures, the best experimental data probably are subject to uncertainties of a few percent, due to the definition and measurement of the wave field. In comparing these measurements with theoretical predictions, additional uncertainties are introduced of the same or larger magnitude, especially due to the role of viscosity. Thus it is impossible to validate a computer program on this basis, with confidence bounds smaller than a few percent.

Since offshore structures are intended for practical service in conditions which depart from the ideal theoretical description, one might argue that it is unnecessary to achieve a high degree of accuracy or confidence in the numerical predictions. However, this argument overlooks the inevitable use of programs in new applications which differ from those where experimental knowledge exists at the time of program development. Ensuring that the program itself is an accurate representation of the theory, to a rationally prescribed tolerance, is a necessary condition for practical use on a variety of present and future problems.

Some guidelines are available from our results to indicate the relationship between the number of panels used to discretize a structure and the resulting accuracy of the hydrodynamic parameters. With careful attention to the discretization, including continuous reduction in the panel width near sharp corners, it appears that reasonable levels of engineering accuracy can be achieved for the structures we have considered, with less than 1000 panels. Finer discretizations are required in special circumstances, for example to analyze a smaller gap width, local variations of the pressure distribution on a structure, or a more complicated geometrical configuration. Generalizations are dangerous, however, and allowances must be made for less systematic discretizations. Routine use of convergence tests is strongly recommended, with substantially finer discretizations employed at selected periods to confirm the accuracy of the results.

From the hydrodynamic standpoint, our results for the catamaran-barge configuration reveal the importance of three-dimensional effects on the resonant gap motions. Not only are the resonant amplitudes reduced, but the periods are shifted significantly below the values predicted by strip theory. The difference between the results for heave and pitch, shown in Figure 5, is an example of the importance of three-dimensional effects and the limitations of strip theory near the resonant period for each mode.

In this paper we have focussed primarily on the first-order effects of the radiation wave forces, and on the free-surface elevation. Various other quantities can be evaluated with the same confidence by the present version of WAMIT, including diffraction effects, exciting forces, body motions, local pressures on the body, the pressure and velocity at field points in the fluid, and the steady horizontal drift forces and yaw moment. An important task which remains is the implementation of a complete second-order solution, including both the sum- and difference-frequency forces acting on a body in a spectrum of waves. This extension will be facilitated by the robust and efficient features of the first-order solution.

9. ACKNOWLEDGEMENTS

Portions of this work were supported by the National Science Foundation, the Office of Naval Research, the David Taylor Research Center, and Veritec A/S. Computational facilities have been provided through an Equipment Grant from the Digital Equipment Corporation, and through the Office of Advanced Scientific Computing of the National Science Foundation.

10. REFERENCES

[1] HESS, J. L. and SMITH, A. M. O., *Calculation of nonlifting potential flow about arbitrary three-dimensional bodies* Douglas Aircraft Co. Report No. E.S. 40622, 1962. (Also in abbreviated form in *J. Ship Res.* 8, 1964.)

[2] EATOCK TAYLOR, R. and JEFFERYS, E. R., "Variability of hydrodynamic load predictions for a tension leg platform" *Ocean Engineering* **13**, 5, 1985, pp. 449-490.

[3] BREIT, S. R., NEWMAN, J. N. and SCLAVOUNOS, P. D., "A new generation of panel programs for radiation-diffraction problems" Conference on the Behaviour of Offshore Structures, 1985, Delft, pp. 531-544.

[4] KORSMEYER, F. T., LEE, C.-H., NEWMAN, J. N. and SCLAVOUNOS, P. D., "The analysis of wave interactions with tension leg platforms" Conference on Offshore Mechanics and Arctic Engineering, ASME, **2**, 1988, Houston, pp. 1-20.

[5] WEHAUSEN, J. V. and LAITONE, E. V., "Surface waves" *Handbuch der Physik*, 9, Springer, Berlin, 1960, pp. 446-778.

[6] BURTON, A. J. and MILLER, G. F., "The application of integral equation methods to the numerical solution of some exterior boundary-value problems" *Proc. Royal Soc. London* **A323**, 1971, pp. 201-220.

[7] LEE, C.-H. "Numerical methods for the solution of three-dimensional integral equations in wave-body interactions" Ph.D. Thesis, Dept. of Ocean Engineering, MIT, 1988.

[8] SCLAVOUNOS, P. D. and LEE, C.-H., "Topics on boundary-element solutions of wave radiation-diffraction problems" 4th International Conf. on Numerical Ship Hydrodynamics, Washington D. C., 1985, pp. 175-184.

[9] LEE, C.-H. and SCLAVOUNOS, P. D., "Removing the irregular frequencies from boundary integral equations in wave body interactions" (Submitted for publication), 1987.

[10] NEWMAN, J. N., "Distributions of sources and normal dipoles over a quadrilateral panel" *J. Eng. Maths.* **20**, 1986, pp. 113-126.

[11] NEWMAN, J. N. "Algorithms for the free-surface Green function" *J. Eng. Maths.* 19, 1985, pp. 57-67.

[12] NEWMAN, J. N. "Interaction of water waves with two closely spaced vertical obstacles" *J. Fluid Mech.* 66, 1974, pp. 97-106.

[13] MARTHINSEN, T. and VINJE, T., "Nonlinear hydrodynamic interaction in offshore loading systems" Conference on the Behaviour of Offshore Structures, 1985, Delft, pp. 293-302.

[14] FOX G., JOHNSON M. A., LYZENGA G. A., OTTO S. W., SALMON J. K. and WALKER D. W. *Solving problems on concurrent processors,* Prentice Hall Publishing Co., in press.

APPENDIX - INTEGRALS OF THE LOGARITHMIC SINGULARITY

If the positions of the source and field point are close to each other and to the free surface, a logarithmic singularity is encountered in the free-surface Green function, analogous to the more singular component inversely proportional to the distance from the field point to the image of the source point above the free surface. In this Appendix we derive expressions for the analytic integration of this logarithmic singularity, and its normal derivative, over a quadrilateral panel. The essential tasks are to evaluate integrals of the form

$$L = \iint_S \psi d\xi d\eta \tag{A.1}$$

$$D = \iint_S \frac{\partial \psi}{\partial \zeta} d\xi d\eta \tag{A.2}$$

where the integrals are over the panel surface. The logarithmic singularity ψ in the free-surface source potential is defined by ([11], equation 5),

$$\psi = \log r(1 + \cos\theta) \tag{A.3}$$

and

$$r = \sqrt{(x-\xi)^2 + (y-\eta)^2 + (z-\zeta)^2} \tag{A.4}$$

Here the Cartesian coordinates (x, y, z) and (ξ, η, ζ) of the image source and field point, respectively, are defined with respect to the panel coordinates, with $z = 0$ the plane of the panel, and θ is the angle between the positive z-axis (normal to the panel) and the (upward) vertical vector $\mathbf{k}$ perpendicular to the plane of the free surface.

The integrals (A.1) and (A.2) can be evaluated in closed form, with the help of some vector analysis. For this purpose we consider a pyramid with the quadrilateral panel as its base and the field point as its vertex. The four sides of this pyramid are triangles bounded by the respective sides of the panel and the rays from the panel vertices to the field point. In the following analysis $\iint_{T_i} dS$ denotes integration over each of the four triangular sides T_i, with the index $i = (1, 2, 3, 4)$. The relations which follow take advantage of the fact that the logarithmic singularity (A.3) is a harmonic function, except at the singular point $r = 0$.

Applying Green's theorem to the harmonic functions ψ and ζ gives the relation

$$\iint_S (\psi\zeta_n - \zeta\psi_n) d\xi d\eta + \sum_{i=1}^{4} L_i = 0 \tag{A.5}$$

where the subscript n denotes normal differentiation and

$$L_i = \iint_{T_i} (\psi\zeta_n - \zeta\psi_n) dS \tag{A.6}$$

Since $\varsigma = 0$ on the panel, the integral in (A.5) is equal to (A.1), and L may be evaluated from the alternative expression

$$L = -\sum_{i=1}^{4} L_i \tag{A.7}$$

Similarly, from the divergence theorem,

$$D = \iint_S \psi_n \, d\xi d\eta = -\sum_{i=1}^{4} D_i \tag{A.8}$$

where

$$D_i = \iint_{T_i} \psi_n \, dS \tag{A.9}$$

In the following analysis of the integrals defined by (A.6) and (A.9), it is sufficient to consider only one triangle, and to use the subscripts 1 and 2 to denote the two corresponding vertices of the panel.

Cartesian coordinates (u, v, w) and corresponding polar coordinates (ρ, α, w) are defined with $w = 0$ in the plane of the triangle, $w > 0$ for the interior domain of the pyramid, and with the origin at the vertex. The triangle is bounded by the rays α_1 and α_2, and by the opposite side. The latter is a straight line in the (u, v) plane between the points (u_1, v_1) and (u_2, v_2). The equation of this straight line can be defined as $Au + Bv = 1$, or equivalently in polar coordinates by

$$\rho(\alpha) = \frac{1}{A\cos\alpha + B\sin\alpha} = \frac{1}{C\cos\beta} \tag{A.10}$$

where the parameters in this equation are defined as follows:

$$A + iB = Ce^{i\delta} = \frac{-v_1 + v_2 + i(u_1 - u_2)}{(u_1 v_2 - u_2 v_1)} \tag{A.11}$$

$$\beta = \alpha - \delta \tag{A.12}$$

It is helpful to rotate the (u, v) plane about the w-axis so that the vertical vector k is in the (u, w) plane, and to define the angle φ between k and the w-axis. It follows that $\cos\theta = -\cos\alpha\sin\varphi$ and, in the plane of the triangle,

$$\psi(\rho, \alpha, 0) = \log\rho(1 - \cos\alpha\sin\varphi) \tag{A.13}$$

The normal derivative in the same plane is

$$\psi_n = \frac{-\cos\varphi}{\rho(1-\cos\alpha\sin\varphi)} \tag{A.14}$$

After making these substitutions in (A.9) and evaluating the resulting integrals with respect to ρ and α in that order, it follows that

$$D_i = \frac{1}{A^2 + B^2\cos^2\varphi}\Bigg[- C\cos\varphi\log(\tan\beta + \sec\beta) + A\sin\varphi\cos\varphi\tan^{-1}\left(\frac{\cos\varphi\sin\alpha}{\sin\varphi - \cos\alpha}\right) + B\cos\varphi\sin\alpha\log\left(\frac{1-\cos\alpha\sin\varphi}{\cos\beta}\right)\Bigg]_1^2 \tag{A.15}$$

Here the subscript and superscript and the last bracket denote evaluations at the corresponding limits α_1 and α_2 of the last integration. [The corresponding values of β follow from (A.12)].

The evaluation of (A.6) is similar, with the final result

$$L_i = -\frac{1}{2}zD_i(1 + \cos\delta\cot\gamma\tan\varphi) - \frac{1}{2}\frac{\cos\gamma}{C^2}\Bigg[- \frac{3}{2}\tan\beta - \sec\varphi\tan^{-1}\left(\frac{\cos\varphi\sin\alpha}{\sin\varphi - \cos\alpha}\right) + \tan\beta\log\left(\frac{1-\cos\alpha\sin\varphi}{C\cos\beta}\right)\Bigg]_1^2 \tag{A.16}$$

where the angle γ, the elevation of the triangle above the quadrilateral plane, is evaluated in the interval $(0, \pi)$.